Structural and magnetic properties of churchite-type REPO4 center dot 2H(2)O materials

M. Rafiuddin, S. Guo, G. Donato, A. Grosvenor, N. Dacheux, R. Cava, A. Mesbah

Structural and Magnetic Properties of Churchite-type $REPO_4 \cdot 2H_2O$ Materials

Mohamed Ruwaid Rafiuddin[1,2*], Shu Guo,[3,†] Giovanni Donato[4], Andrew P. Grosvenor[4], Nicolas Dacheux[1], Robert. J. Cava[3] and Adel Mesbah[1,5,*]

[1]ICSM, Univ Montpellier, CEA, CNRS, ENSCM, Marcoule, France

[2]MIAMI Irradiation Facility, School of Computing and Engineering, University of Huddersfield, HD1 3DH, UK

[3]Department of Chemistry, Princeton University, Princeton, New Jersey 08544, United States

[4]Department of Chemistry, University of Saskatchewan, Saskatoon, Saskatchewan, Canada S7N 5C9

[5] Univ Lyon, Université Lyon 1, Institut de Recherches sur la Catalyse et l'Environnement de Lyon, IRCELYON, UMR5256, CNRS, 2 Avenue Albert Einstein, 69626, Villeurbanne Cedex, France

*Corresponding Authors

M.Rafiuddin@hud.ac.uk

Adel.mesbah@irecelyon.univ-lyon1.fr

Abstract

The structural and magnetic properties of Churchite-type $REPO_4 \cdot 2H_2O$ (RE = Gd to Lu) materials (low-temperature polymorph of the rare-earth phosphate family) are reported. The materials were synthesized at low temperatures (4°C) using a precipitation method and the long-range and local structures were determined using powder XRD and XANES. The Churchite materials crystallize in the monoclinic system (Space group – *C*2/*c*) and adopt a 2D layered structure with water occupying the interlayer regions. The churchite materials were found to transform to the xenotime structure at 300ºC. DC magnetization experiments reveal the absence of long-range magnetic ordering between 300 and 1.8 K. The effective magnetic moments (μ_{eff}) are similar to those of the free RE (RE = Gd, Tb, Dy, Ho, Er) ions.

1. Introduction

Rare-earth phosphates belong to a unique class of materials with rich structural chemistry and owing to this, these materials have wide-ranging applications in fields such as photonics, catalysis, radioactive waste management, and biomedical imaging.[1–4] These materials, depending on the synthetic conditions, can crystallize in the following structure-types: Monazite ($REPO_4$; RE = La-Gd; Space group = $P2_1/n$), Xenotime ($RE'PO_4$; RE = Tb-Lu & Y; Space group = $I4_1/amd$), Rhabdophane ($REPO_4 \cdot H_2O$; RE = La-Dy; Space group – $C2$), and Churchite ($REPO_4 \cdot 2H_2O$; RE = Gd-Lu & Y; Space group – $C2/c$).[5–7] Studies discussing the synthetic and structural aspects of rare-earth phosphates have been reported in the literature.[8–11] Similarly, reports on the optical properties, radiation-resistance, and chemical durability of rare-earth phosphates can also be found in the literature.[12–19]

The presence of rare-earth (RE) ions can give rise to interesting magnetic properties, thereby enabling the use of rare-earth phosphates as a contrast agent in magnetic resonance imaging (MRI) applications. [20,21] However, the magnetic properties of rare-earth phosphates have not been reported in detail, and to the best of our knowledge, only few reports have been published. In one of the earliest reports, Saji et al. determined the magnetic properties of rare-earth phosphates and vanadates, RXO_4 (R = Pr, Nd, Sm, Eu, Gd, Tb, Dy, Ho, Er and Yb; X = P and V) adopting the monazite and xenotime structures.[22] It was shown in that study that the RE^{3+} cations predominantly gave rise to the magnetic moments observed in this material and that the temperature dependent magnetizations of these materials obeyed the Curie-Weiss law above 200 K.[22]. In a study by Cook et al., the magnetic properties of xenotime-type $HoPO_4$ were determined, and it was reported that $HoPO_4$ undergoes a transition to an antiferromagnetic state at a Neel temperature of 1.39 K.[23]. In a recent study by Kumar et al., the magnetic properties

of monazite-type Nd^{3+} doped $GdPO_4$ were determined, and it was shown that the material exhibits paramagnetic behaviour and was attributed to the presence of paramagnetic Gd^{3+} ions.[24].

In the current study, the Churchite materials ($REPO_4 \cdot 2H_2O$; RE = Gd - Lu) were synthesized using a low temperature precipitation route and the structures were analyzed using powder XRD and X-ray absorption near-edge spectroscopy (XANES). The temperature dependent magnetic susceptibilities of $REPO_4 \cdot 2H_2O$ (RE = Gd, Tb, Dy, Ho, Er) materials were measured between 300 and 1.8 K and the effective magnetic moments and the Curie-Weiss temperatures were determined. To the best of our knowledge, the local structure and magnetic properties of Churchite-type rare-earth phosphates have not been previously reported and this study aims to fill this literature gap.

2. Experimental

2.1. Synthesis

Churchite-type $REPO_4 \cdot 2H_2O$ materials were synthesized using a previously reported synthetic procedure.[7] The following precursors were used: $GdCl_3 \cdot 6H_2O$ (Sigma-Aldrich; 99%), $TbCl_3 \cdot 6H_2O$ (Sigma-Aldrich; 99.9%), $DyCl_3 \cdot 6H_2O$ (Sigma-Aldrich; 99.99%), $HoCl_3$ (Sigma-Aldrich; 99.9%), $ErCl_3 \cdot nH_2O$ (Sigma-Aldrich; 99.9%), $TmCl_3$ (Sigma-Aldrich; 99.9%), $YbCl_3$ (Sigma-Aldrich; 99.9%), $LuCl_3$ (Sigma-Aldrich; 99.9%), H_3PO_4 (85% Normapur), and HCl (37% Carbo Erba). The rare-earth chloride salts were dissolved in 1M HCl and the concentration of the final solution was determined using ICP-AES. The concentration of the RE ions varied between 0.5M and 1M. The rare-earth chloride solution was added to a 5M H_3PO_4 solution (with an excess of 3 mol%) and stirred for a few hours before placing the solution mixture in a fridge

(4°C) for 24 months. Crystalline powders settled at the bottom of the container and the powders were recovered by centrifugation and washed twice with water and once with ethanol. The powders were then dried in air at room-temperature. To monitor the temperature-induced changes in the structure of $REPO_4.2H_2O$ materials, powders of $LuPO_4 \cdot 2H_2O$ were heated to 300°C and 1000°C for 2 hours in air (Heating rate of 100°C/h) followed by cooling to room temperature with a rate of 150°C/h.

2.2. Powder X-ray Diffraction

Powder XRD measurements were carried out using a Bruker D8-Advance diffractometer equipped with a Cu $K_{\alpha 1,2}$ radiation (λ = 1.5418 Å). The powder XRD patterns of the as-synthesized $REPO_4 \cdot 2H_2O$ and annealed $LuPO_4$ samples were collected from 5° to 100° using step size of 0.0167° and a total time of 3 hours per sample. Rietveld refinements of the as-synthesized $REPO_4 \cdot 2H_2O$ materials were determined using a Profex (version 4.3.3) software.[25] During the refinement, the lattice constants, isotropic thermal displacement parameters of RE and P ions were allowed to vary. The atomic coordinates and site occupancy factors were fixed during the refinement.

2.3. XANES

2.3.1. P $L_{2,3}$-edge XANES

The P $L_{2,3}$-edge XANES spectra were collected from as-synthesized ($ErPO_4 \cdot 2H_2O$, $HoPO_4 \cdot 2H_2O$, $LuPO_4 \cdot 2H_2O$) and annealed $LuPO_4$ (300°C and 1000°C) materials using the Variable Line Spacing – Plane Grating Monochromator (VLS-PGM; 11ID-2) beamline at the Canadian Light Source, CLS (Saskatoon, Canada).[26] The P $L_{2,3}$-edge spectra were collected

using a high-energy grating monochromator and the resolution of the spectra at the P L_3-edge is 0.01 eV. Fine powders of $ErPO_4 \cdot 2H_2O$ and $HoPO_4 \cdot 2H_2O$ were placed on carbon tape, and the spectra was collected under vacuum in a total fluorescence yield mode using a step size of 0.05 eV. The calibration of the P $L_{2,3}$-edge spectra were done using a spectrum collected from Red P and choosing the maximum in the first derivative curve to 130 eV. All the XANES spectra discussed in this study were analyzed using the Athena software program.[27]

2.3.2. Lu L_1-edge XANES

Lu L_1-edge XANES spectra were collected from as-synthesized $LuPO_4 \cdot 2H_2O$ and annealed $LuPO_4$ samples (300°C and 1000°C) using the Sector 20 - bending magnet (BM) beamline located at the Advanced Photon Source (APS; Argonne National Laboratory).[28] All the spectra were collected using a Si (111) double crystal monochromator in the transmission mode and the ionization chambers were filled with 100% N_2. The spectral resolution of the Lu L_1-edge spectra at the Lu L_1-edge (10870 eV) is 1.5 eV. Powders of as-synthesized and annealed samples were placed on a Kapton tape and the spectra was collected using a step size of 0.15 eV through the Lu L_1-edge. The Lu L_1-edge spectra was calibrated using a Ga metal foil (Ga K-edge energy = 10367 eV) placed in between the transmission (I_t) and reference ionization chambers (I_{ref}).

2.4. Magnetic Measurements

Temperature-dependent magnetizations (M) were measured on powder samples of approximate weight 0.1 g between 1.8 and 300 K in an applied field (H) of 2000 Oe on a Quantum Design PPMS (Physical Property Measurement System) Dynacool. Susceptibility was defined as M/H. Measurements were made in the DC mode, using the vibrating sample magnetometer function.

The field-dependent magnetization of $REPO_4 \cdot 2H_2O$ (RE = Gd, Tb, Dy, Ho, Er) were collected at 2 K.

3. Results and Discussion

3.1. Crystal structure and Local structure of $REPO_4 \cdot 2H_2O$ materials

The PXRD patterns of the as-synthesized $REPO_4 \cdot 2H_2O$ (RE = Gd - Lu) materials indicate that they are phase-pure and crystallize in the monoclinic crystal system (Space group: *C*2/*c*) (Figure 1a).[29] Rietveld refinement was performed on one of the members of the churchite series ($LuPO_4 \cdot 2H_2O$) using the churchite-type $YPO_4 \cdot 2H_2O$ structural model proposed by Ivashkevich et al and the results indicate a good match with the experimental and calculated PXRD patterns (Figure 1b).[29] The crystallographic data of refined $LuPO_4 \cdot 2H_2O$ is presented in Table 1. It can be observed in Figure 1a that the diffraction peaks consistently shift to higher 2θ on moving from $GdPO_4 \cdot 2H_2O$ to $LuPO_4 \cdot 2H_2O$ and is a result of the decrease in the ionic radii of RE^{3+} ions. Consistent with the shift in the diffraction peaks, the lattice constants of $REPO_4.2H_2O$ also decrease on moving from $GdPO_4 \cdot 2H_2O$ to $LuPO_4 \cdot 2H_2O$ thereby indicating the contraction of the unit cell (Table 2). The crystal structure of Churchite-type $REPO_4 \cdot 2H_2O$ is shown in Figure 2.[29] In this structure, the RE^{3+} ions are coordinated to eight oxygen atoms and the resulting REO_8 polyhedra adopts a distorted square antiprism geometry; in the REO_8 polyhedra, the six oxygen atoms are provided by the phosphate groups and two oxygen atoms are provided by the water molecules. The REO_8 polyhedra are connected to each other via PO_4 tetrahedra, resulting in the formation of 1D chains along the [100] direction. These 1D chains are in turn connected to each other via edge-sharing of the REO_8 polyhedra and this results in the formation of 2D layers. These 2D layers are stacked along the *b*-axis and the space between the 2D layers is occupied by water molecules.

The local structure of P in the Churchite materials was determined by collecting the P $L_{2,3}$-edge XANES spectra (Figure 3). In those spectra, X-ray induced electronic transitions occur from the P 2*p* state into the P 3*s* and P 3*d* conduction states. In Figure 3, however, the various spectral features are attributed to an electronic transition from the P 2*p* state into overlapping P 3*s* and P 3d conduction states.[9,30] The spectral line shape of the materials investigated in this study are similar, an indication that all the $REPO_4 \cdot 2H_2O$ (RE = Ho, Er, Tm, Lu) materials adopt the Churchite structure (Figure 3). Similarly, the local structure of RE in the Churchite materials were determined in this study via collection of Lu L_1-edge spectra from Churchite-type $LuPO_4 \cdot 2H_2O$ (Figure 4). The Lu L_1-edge spectra consists of a weak pre-edge shoulder (2s → 6p-5d) and a strong main-edge (2s → 6p) peak (Figure 4).[31–33] The pre-edge shoulder is possible due to the distorted square antiprism geometry of the LuO_8 polyhedra which therefore allows for the hybridization of the 6*p* and 5*d* states. It can be observed from Figures 3 and 4 that the P $L_{2,3}$- and Lu L_1-edge spectra are structurally rich and display many features in the near-edge region thereby making them useful probes to monitor the changes in the local structure of materials with increasing temperature.

3.2. Effect of temperature on the long-range and local structure

In a previous study, it was shown using thermogravimetry (TGA) that Churchite materials lose structural water between 200°C - 300°C and that the powder XRD patterns of the post TGA samples (that were heated to 1000°C) revealed the structural transformation to the xenotime structure.[7] However, it is unknown whether the structural transformation is direct or whether it proceeds via an anhydrous Churchite structure intermediate. To address this question, one of the members of the churchite series ($LuPO_4 \cdot 2H_2O$) was annealed at both 300°C and 1000°C in air.

The ex-situ ambient temperature powder XRD patterns of the annealed materials are shown in Figure 5. Upon heating to 300°C, the data show that the Churchite structure is not stable and transforms directly to the xenotime (*I*4$_1$/*amd*) structure; an anhydrous Churchite structure intermediate is not observed. The crystal structure of xenotime-type $LuPO_4$ is shown in Figure 6. It is interesting to note that the rhabdophane-type material $SmPO_4 \cdot 0.667H_2O$, which also contains structural water, loses water in two steps, each step being associated with a structural transformation.[34] In the first (at ~80°C) and the second (at ~213°C) steps of water loss for that material, rhabdophane ($SmPO_4 \cdot 0.667H_2O$) undergoes a structural transformation to hemihydrate ($SmPO_4 \cdot 0.5H_2O$) and anhydrous ($SmPO_4$) phases, respectively.[34] It should be noted that the anhydrous rhabdophane structure is stable up to ~500°C and beyond that temperature undergoes a structural transformation to the monazite structure.[34] In the current study, after heating the Lu-Churchite at 300°C, the diffraction peaks are broad and is due to the small size of xenotime crystallites (Figure 5). At 1000°C, the diffraction peaks sharpen due to an increase in the crystallite size (Figure 5). The lattice constants of the as-synthesized $LuPO_4 \cdot 2H_2O$ and annealed $LuPO_4$ materials are provided in Table 3.

The changes in the local structure of Churchite materials was determined as a function of temperature by collecting the P $L_{2,3}$-edge and Lu L_1-edge XANES spectra of as-synthesized $LuPO_4 \cdot 2H_2O$ and annealed $LuPO_4$ (300°C, 1000°C) materials (Figures 7 and 8). In the P $L_{2,3}$-edge spectra, a distinct change in the spectral line shape and a shift in the near-edge is observed for the material annealed at 300°C and 1000°C (Figure 7). This observation indicates that the local structure around the P atom in the material that has been heated to 300°C and 1000°C is different in comparison to the as-synthesized Churchite-type $LuPO_4 \cdot 2H_2O$ material and is

attributed to the structure transformation from the Churchite to xenotime structure. The change in lineshape can be explained by comparing the P – O bond distances of the PO_4 tetrahedra in churchite and xenotime structures. Churchite-type $LuPO_4 \cdot 2H_2O$ has a slightly distorted PO_4 tetrahedra (P – O bond length = 1.506Å – 1.516Å) in comparison to the PO_4 tetrahedra of xenotime-type $LuPO_4$ (P – O bond length = 1.534Å; See Table 4). As a result, the P $L_{2,3}$-edge spectra of churchite-type $LuPO_4 \cdot 2H_2O$ has a less pronounced fine structure at the near edge (Figure 7). Upon heating the $LuPO_4 \cdot 2H_2O$ material to 300°C and 1000°C, the churchite structure transforms to the xenotime structure. This structural transformation is reflected in the P $L_{2,3}$-edge spectra in the form of a more pronounced fine structure at the near-edge region and is a result of the symmetrical nature of the PO_4 tetrahedra in the xenotime structure (Figure 7).

In the Lu L_1-edge spectra of the materials annealed at 300°C and 1000°C, the near-edge region becomes narrower and a slight increase in the intensity of the main-edge peak is observed in comparison to as-synthesized $LuPO_4 \cdot 2H_2O$ (Figure 8). The change in the Lu L_1-edge spectral lineshape as a function of temperature can also be explained by comparing the Lu-O bond distances in the churchite and xenotime structures (See Table 4). The LuO_8 polyhedra in churchite (Lu – O = 2.258Å – 2.446Å) is more distorted in comparison to the LuO_8 polyhedra in the xenotime (Lu – O = 2.257Å and 2.344Å). Thus, the changes in the local symmetry of LuO_8 polyhedra is reflected in the form of changes in the intensity of the Lu L_1 main-edge peak of churchite-type $LuPO_4 \cdot 2H_2O$ and xenotime-type $LuPO_4$. Upon heating $LuPO_4 \cdot 2H_2O$ to 300°C and 1000°C, the intensity of the main-edge peak in the Lu L_1-edge spectra increases and indicates a structure transformation from churchite (LuO_8 - square antiprism geometry) to xenotime (LuO_8 – dodecahedron geometry) structure (Figure 8). [7,35]

3.3. Magnetic Properties of $REPO_4 \cdot 2H_2O$ materials

To reveal the magnetic properties of *RE*$PO_4 \cdot 2H_2O$ (*RE* = Gd, Tb, Dy, Ho, and Er), Curie-Weiss fits were applied to the inverse susceptibilities, based on the formula $\chi - \chi_0 = C/(T - \Theta)$ where χ refers to the measured susceptibility, χ_0 is the temperature independent contribution to the susceptibility (negligible in these cases), C is the Curie Constant and Θ is the Curie-Weiss temperature. $\mu_{\text{eff}} = \sqrt{8C}$ is used for calculating the effective magnetic moments.

As shown in Figure 9, long range magnetic ordering is absent down to 1.8 K, according to the DC magnetization data for all tested members in the $REPO_4 \cdot 2H_2O$ family. For $GdPO_4 \cdot 2H_2O$, a nice Curie-Weiss fitting was applied in the high temperature range (150-280 K), which gives a small negative Weiss temperature Θ = -0.1 K and effective magnetic moment μ_{eff} = 7.83 μ_B/Gd for $GdPO_4 \cdot 2H_2O$ (Figure 9a). The value of effective moment is in a good agreement with the expected value of the free ion for Gd (7.94 μ_B/Gd). The small Weiss temperature implies weak magnetic interaction for $GdPO_4 \cdot 2H_2O$. Similar Curie-Weiss fittings were also performed for the other members (Figure 9b – 9e) in the high-temperature regime. The Weiss temperature Θ and effective magnetic moment μ_{eff} for the studied materials are summarized in Table 5. The Weiss temperatures for $TbPO_4 \cdot 2H_2O$, $DyPO_4 \cdot 2H_2O$, $HoPO_4 \cdot 2H_2O$, $ErPO_4 \cdot 2H_2O$ are -7.4 K, -8.5 K, -9.5 K, and -10.1 K, respectively. These values are relatively large compared with Θ = -0.1 K for $GdPO_4.2H_2O$. The effective moments for $TbPO_4 \cdot 2H_2O$, $DyPO_4 \cdot 2H_2O$, $HoPO_4 \cdot 2H_2O$, $ErPO_4 \cdot 2H_2O$ are close to the expected values of the free ion for RE (Table 5 and Figure 10). The relationship between polycrystalline Curie–Weiss temperatures Θ of *RE*$PO_4 \cdot 2H_2O$ and de Gennes factor *d*G (*d*G = $(g_J\text{-}1)^2\ J(J\text{+}1)$) is depicted in Figure 10 (right), where *g* refers to Lande splitting factor and *J* is the total angular momentum.

The isothermal magnetization $M(H)$ curves at 2 K for $RE PO_4 \cdot 2H_2O$ are shown in Figure 11 - hysteresis loops were absent for these materials and nonlinear M versus H behavior were observed in the field-dependent magnetization of all members at 2 K. For the Gd- and Tb-samples, the $M(H)$ curves saturates at ~6.76 μ_B (Gd) and ~4.93 μ_B (Tb), respectively for the applied field of $\mu_0 H$ = 9 T. Nonlinear responses were observed for other members; however, saturations were not found up to μ_0H = 9 T in the $M(H)$ curves for Ln = Dy, Ho, and Er.

To facilitate the comparison, the normalization of the temperature dependent susceptibilities of $RE PO_4 \cdot 2H_2O$ (*RE* = Gd, Tb, Dy, Ho, and Er) are depicted in Figure 12. This figure supports the nicely paramagnetic behavior of this family of materials over a wide temperature range. The divergences for some of the materials at low temperatures ($T/|\Theta| < 2$) (Figure 12, inset) are likely attributed to crystal electric field (CEF) effects. The anomalous behavior displayed by the Ho material suggests that it may be heading for a transition where lower magnetic moment is observed, just below the temperature range of our measurements, and thus it may be suitable for future study. Due to the relatively localized 4*f* electrons of the rare earth elements, the magnetic interactions are weak and further experiments (ultralow temperature specific heat, ultralow temperature AC susceptibilities, and neutron scattering for example) would be needed to reveal the magnetic ground states of all these materials.

4. Conclusion

Materials adopting the Churchite-type structure ($REPO_4 \cdot 2H_2O$; Space group: *C*2/*c*) were synthesized using a low-temperature precipitation method. The materials were found to be stable over a narrow temperature range (T < 300°C). At temperatures 300°C and above, they transform into the xenotime structure. Distinct changes in the local structure of P and RE (RE = Lu) ions were observed in the P $L_{2,3}$-edge and Lu L_1-edge spectra of as-synthesized $LuPO_4 \cdot 2H_2O$ and

annealed $LuPO_4$ materials. The magnetic properties of the as-synthesized $REPO_4 \cdot 2H_2O$ materials were determined via Field-dependent Magnetization, and Temperature-dependent Susceptibility measurements. None of the members of the Churchite series investigated in this study were found to display long-range magnetic ordering down to 1.8 K. The effective magnetic moments (μ_{eff}) of all the $REPO_4 \cdot 2H_2O$ materials were found to be similar to those of free RE (RE = Gd, Tb, Dy, Ho, Er) ions. Field dependent magnetization measurements at 2 K revealed the absence of hysteresis loop and the existence of a non-linear M vs H relationship in these materials. This study reported, for the first time, the variations in the local structure of Churchite-type $REPO_4 \cdot 2H_2O$ materials as a function of temperature in addition to determining the magnetic properties of the $REPO_4 \cdot 2H_2O$ materials.

AUTHOR INFORMATION

Corresponding Authors

Adel MESBAH

Univ Lyon, Université Lyon 1, Institut de Recherches sur la Catalyse et l'Environnement de Lyon, IRCELYON, UMR5256, CNRS, 2 Avenue Albert Einstein, 69626, Villeurbanne Cedex, France

Email: adel.mesbah@ircelyon.univ-lyon1.fr

orcid.org/0000-0002-6905-2402

Mohamed Ruwaid Rafiuddin

ICSM, Univ Montpellier, CEA, CNRS, ENSCM, Marcoule, France

MIAMI Irradiation Facility, School of Computing and Engineering, University of Huddersfield, HD1 3DH, UK

Email: M.Rafiuddin@hud.ac.uk

orcid.org/0000-0002-0190-1092

Shu Guo

Department of Chemistry, Princeton University, Princeton, New Jersey 08544, United States

Present address: Shenzhen Institute for Quantum Science and Engineering, Southern University of Science and Technology, Shenzhen, 518055, China

Giovanni Donato, Andrew P. Grosvenor

Department of Chemistry, University of Saskatchewan, Saskatoon, Saskatchewan, Canada S7N 5C9

Nicolas Dacheux[1],

ICSM, Univ Montpellier, CEA, CNRS, ENSCM, Marcoule, France

Robert. J. Cava

Department of Chemistry, Princeton University, Princeton, New Jersey 08544, United States

Notes

The authors declare no competing financial interest

Acknowledgements

The authors would like to thank the French National Research Agency (ANR JCJC-X-MAS; Project # ANR-17-CE06-0004) for the financial support. The P $L_{2,3}$-edge XANES spectra was collected at the VLS-PGM beamline (1ID-2), Canadian Light Source, a national research facility of the University of Saskatchewan, which is supported by the Canada Foundation for Innovation (CFI), the Natural Sciences and Engineering Research Council (NSERC), the National Research Council (NRC), the Canadian Institutes of Health Research (CIHR), the Government of Saskatchewan, and the University of Saskatchewan. The Lu L_1-edge XANES spectra was collected at the 20 BM beamline (CLS@APS Sector 20, APS). Sector 20 facilities at the Advanced Photon Source, and research at these facilities, are supported by the U.S. Department of Energy - Basic Energy Sciences, the Canadian Light Source and its funding partners, and the Advanced Photon Source. Use of the Advanced Photon Source, an Office of Science User Facility operated for the U.S. Department of Energy (DOE) Office of Science by Argonne

National Laboratory, was supported by the U.S. DOE under Contract No. DE-AC02-06CH11357. The beamline staff at the VLS-PGM beamlines in CLS and the Sector 20 BM beamlines at the APS are thanked for their support during beamtime. M. R. Rafiuddin also thanks the Engineering and Physical Sciences Research Council for funding under grants, EP/T012811/1. The magnetic data collection and analysis were supported by the US Department of Energy, Division of Basic Energy Sciences, grant number DE-SC0019331.

Tables

Table 1

Crystal Data	**$LuPO_4 \cdot 2H_2O$**
Formula Weight	305.97
Crystal System	Monoclinic
Space group	*C*2/*c*
Unit cell dimensions a (Å)	 6.0888 (1)
b (Å)	14.8592 (3)
c (Å)	5.5305 (1)
β (º)	115.801 (1)
Unit cell volume ($Å^3$)	450.49 (1)
Z *Theoretical density*	4 4.510
Fit results	$R_p = 0.0256$ $R = 0.0381$ $R_{wp} = 0.0347$ $R_{exp} = 0.0172$ $\chi^2 = 4.07$

Crystallographic data of $LuPO_4 \cdot 2H_2O$

Table 2: Lattice constants of the Churchite phases $LnPO_4 \cdot 2H_2O$

Compound	**a (Å)**	**b (Å)**	**c (Å)**	**β (°)**	**Volume (Å)**
$GdPO_4 \cdot 2H_2O$	6.2062 (1)	15.1148(1)	5.6165 (1)	114.94 (1)	477.69(1)
$TbPO_4 \cdot 2H_2O$	6.1840 (1)	15.0382 (2)	5.6015 (1)	115.05 (1)	471.90(1)
$DyPO_4 \cdot 2H_2O$	6.1650 (1)	15.0201 (1)	5.5910 (1)	115.27 (1)	468.15(1)
$HoPO_4 \cdot 2H_2O$	6.1441 (1)	14.9842 (1)	5.5711 (1)	115.34 (1)	463.54(1)
$ErPO_4 \cdot 2H_2O$	6.1280 (1)	14.9544 (1)	5.5631 (1)	115.48 (1)	460.20(1)
$TmPO_4 \cdot 2H_2O$	6.1144 (1)	14.9088 (1)	5.5539 (1)	115.53 (1)	456.83(1)
$YbPO_4 \cdot 2H_2O$	6.0978 (1)	14.8741 (1)	5.5407 (1)	115.65 (1)	452.99(1)
$LuPO_4 \cdot 2H_2O$	6.0888 (1)	14.8592 (3)	5.53047 (8)	115.801 (1)	450.49 (1)

Table 3: Lattice constants of as-synthesized $LuPO_4 \cdot 2H_2O$ and annealed $LuPO_4$ materials

Compounds	**a**	**b**	**c**	**β**	**Volume (Å)**	**Structure**
As-synthesized	6.0888 (1)	14.8592 (3)	5.53047 (8)	115.801 (1)	450.487 (4)	Churchite
300°C	6.797 (2)		5.966 (2)		275.6 (3)	Xenotime
1000°C	6.7944 (2)		5.9575 (3)		275.0 (2)	Xenotime

Table 4: Refined bond distances of $LuPO_4 \cdot 2H_2O$ (Churchite) and $LuPO_4$ (Xenotime)

Compounds	**P – O bond distance (Å)**	**Lu – O bond distance (Å)**
$LuPO_4 \cdot 2H_2O$ (Churchite)	P – O1 = 1.516 (5) P – O2 = 1.506 (5) P – O3 = 1.516 (5) P – O4 = 1.506 (5)	Lu – O3 = 2.303 (4) Lu – O1 = 2.399 (5) Lu – O2 = 2.446 (4) Lu – O2 = 2.258 (4) Lu – O2 = 2.258 (4) Lu – O3 = 2.303 (4) Lu – O1 = 2.399 (5) Lu – O2 = 2.446 (4)
$LuPO_4$ (Xenotime)	4 × (P – O1) = 1.534	4 × (Lu – O1) = 2.257 (3) 4 × (Lu – O1) = 2.344 (3)

Table 5. Sample information, De Gennes factor, dG = $(g_J - 1)^2 J(J+1)$, temperature independent contribution (χ_0), Effective moments (μ_{eff}), and Weiss temperatures (Θ) determined by fitting of the Curie–Weiss law to the magnetic susceptibility data. μ_{fi} = free ion magnetic moment.

RE	**Mass(mg)**	**dG**	**High*T* fit** (K)	χ_0	μ_{eff} (μ_B)	Θ (K)	μ_{fi} (μ_B)
Gd	16.8	15.75	150-280	-5.13×10^{-4}	7.83	-0.1	7.94
Tb	16.7	10.50	150-280	-4.77×10^{-5}	9.69	-7.4	9.72
Dy	23.7	7.08	150-280	-2.08×10^{-5}	10.52	-8.5	10.63
Ho	18.5	4.50	150-280	-2.59×10^{-4}	10.58	-9.7	10.60
Er	21.3	2.55	150-280	-2.43×10^{-4}	9.56	-10.1	9.58

Figure Captions

Figure 1 – a) Normalized PXRD patterns of as-synthesized Churchite-type $REPO_4 \cdot 2H_2O$ (RE = Gd - Lu) materials. (b) Rietveld refined PXRD pattern of $LuPO_4 \cdot 2H_2O$

Figure 2 – Crystal structure of Churchite-type $REPO_4 \cdot 2H_2O$. The crystal structure was generated using the VESTA software program.

Figure 3 – Normalized P $L_{2,3}$-edge XANES spectra of as-synthesized churchite-type $REPO_4 \cdot 2H_2O$ (RE = Ho, Er, Tm, Lu) materials.

Figure 4 – Lu L_1-edge XANES spectra of as-synthesized churchite type $LuPO_4 \cdot 2H_2O$ material.

Figure 5 – PXRD patterns of as-synthesized $LuPO_4 \cdot 2H_2O$ and heated (300°C, 1000°C) $LuPO_4$ materials.

Figure 6 - Crystal structure of Xenotime-type $LuPO_4 \cdot 2H_2O$. The crystal structure was generated using the VESTA software program.

Figure 7 – P $L_{2,3}$-edge XANES spectra of as-synthesized $LuPO_4 \cdot 2H_2O$ and heated (300°C, 1000°C) $LuPO_4$ materials.

Figure 8 – Lu L_1-edge XANES spectra of as-synthesized $LuPO_4 \cdot 2H_2O$ and heated (300°C, 1000°C) $LuPO_4$ materials.

Figure 9 - Temperature-dependence of the magnetic susceptibilities (blue) and inverse magnetic susceptibilities (orange) of $REPO_4 \cdot 2H_2O$ (RE = Gd, Tb, Dy, Ho, Er).

Figure 10. Changes of effective magnetic moments, free R^{3+} ion moment, and Weiss temperatures (Θ) as a function of de Gennes factor: $(g_J - 1)^2 J(J+1)$. data for $RE PO_4 \cdot 2H_2O$ (R = Gd, Tb, Dy, Ho, and Er).

Figure 11. Field-dependent magnetization for $RE PO_4 \cdot 2H_2O$ (RE = Gd, Tb, Dy, Ho, and Er) at 2 K.

Figure 12. Normalization and comparison of the temperature dependent susceptibilities of $RE PO_4 \cdot 2H_2O$ (R = Gd, Tb, Dy, Ho, and Er). Inset shows the behavior for normalized temperatures below $T/|\Theta| = 2$.

Figures

Figure 1

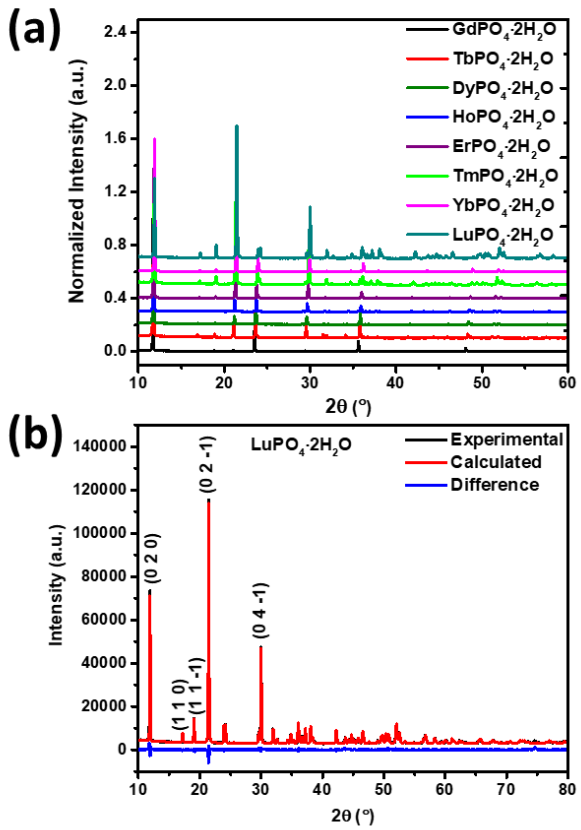

Figure 2

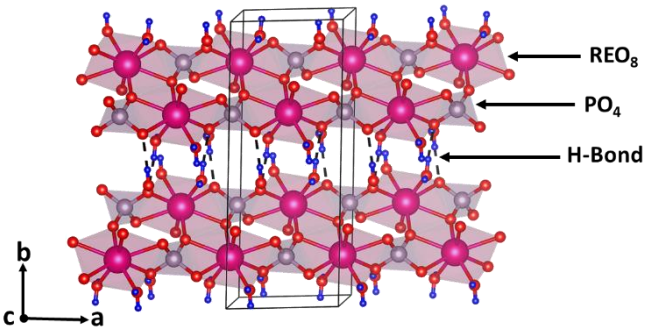

Figure 3

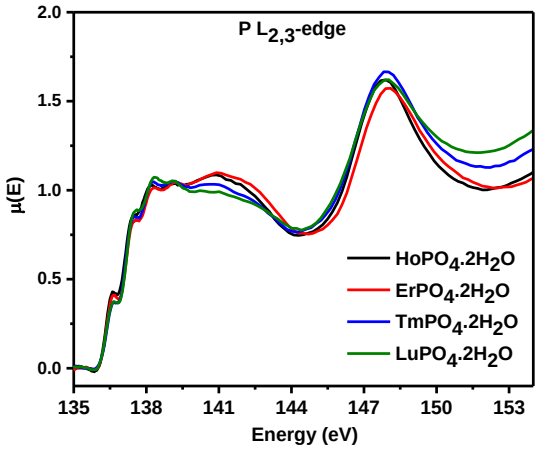
P L2,3-edge
μ(E)
Energy (eV)
2.0
1.5
1.0
0.5
0.0
135
138
141
144
147
150
153
HoPO4.2H2O
ErPO4.2H2O
TmPO4.2H2O
LuPO4.2H2O

Figure 4

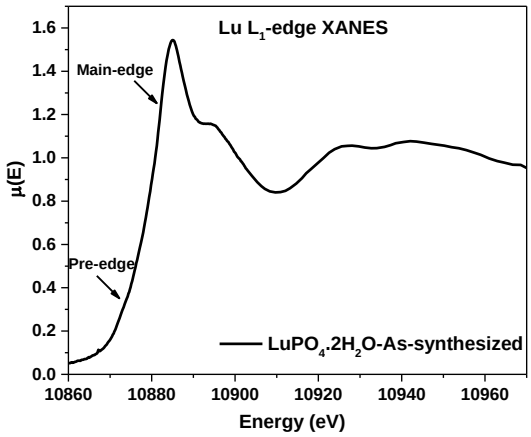
Lu L1-edge XANES
Main-edge
Pre-edge
μ(E)
Energy (eV)
LuPO4.2H2O-As-synthesized
1.6
1.4
1.2
1.0
0.8
0.6
0.4
0.2
0.0
10860
10880
10900
10920
10940
10960

Figure 5

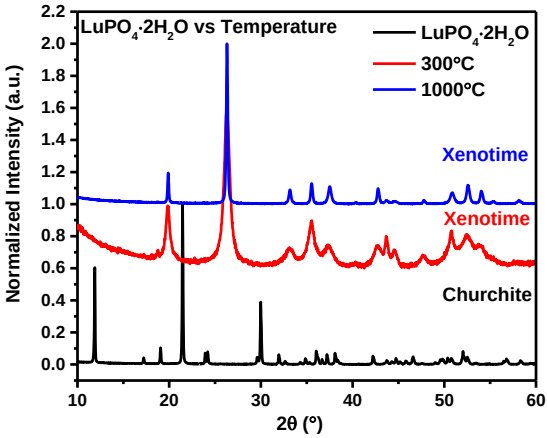
LuPO4·2H2O vs Temperature
LuPO4·2H2O
300°C
1000°C
Xenotime
Xenotime
Churchite
Normalized Intensity (a.u.)
2θ (°)
0.0
0.2
0.4
0.6
0.8
1.0
1.2
1.4
1.6
1.8
2.0
2.2
10
20
30
40
50
60

Figure 6

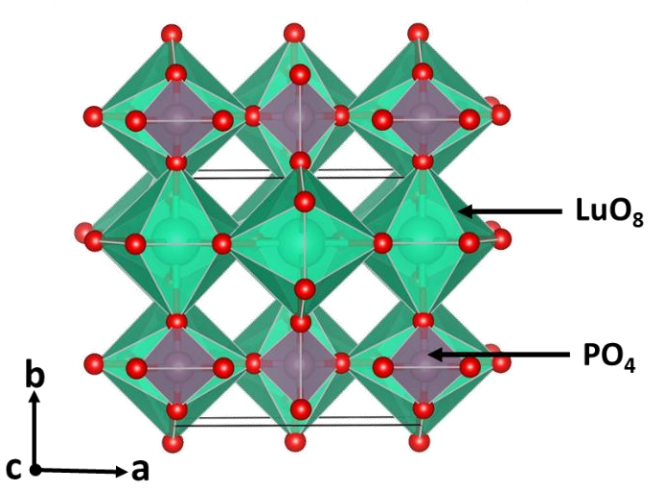

Figure 7

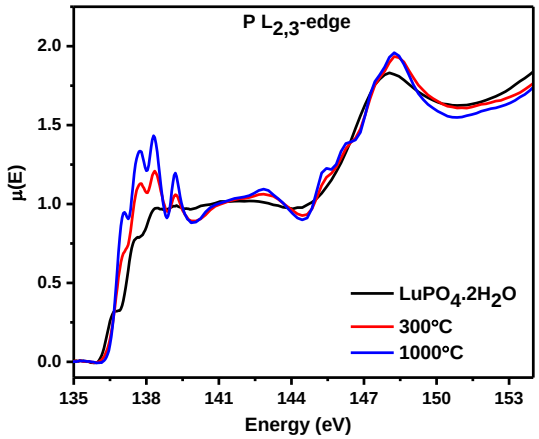

Figure 8

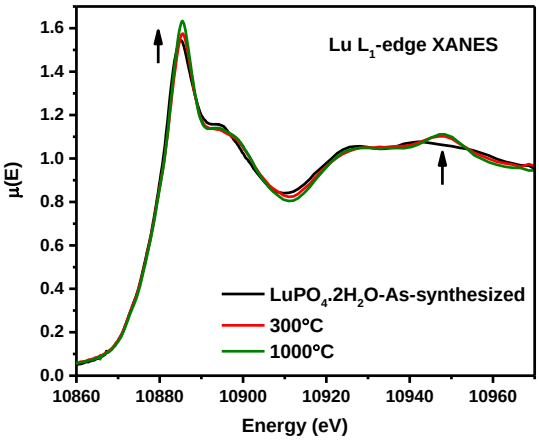
Lu L1-edge XANES
μ(E)
Energy (eV)
LuPO4.2H2O-As-synthesized
300°C
1000°C
1.6
1.4
1.2
1.0
0.8
0.6
0.4
0.2
0.0
10860
10880
10900
10920
10940
10960

Figure 9

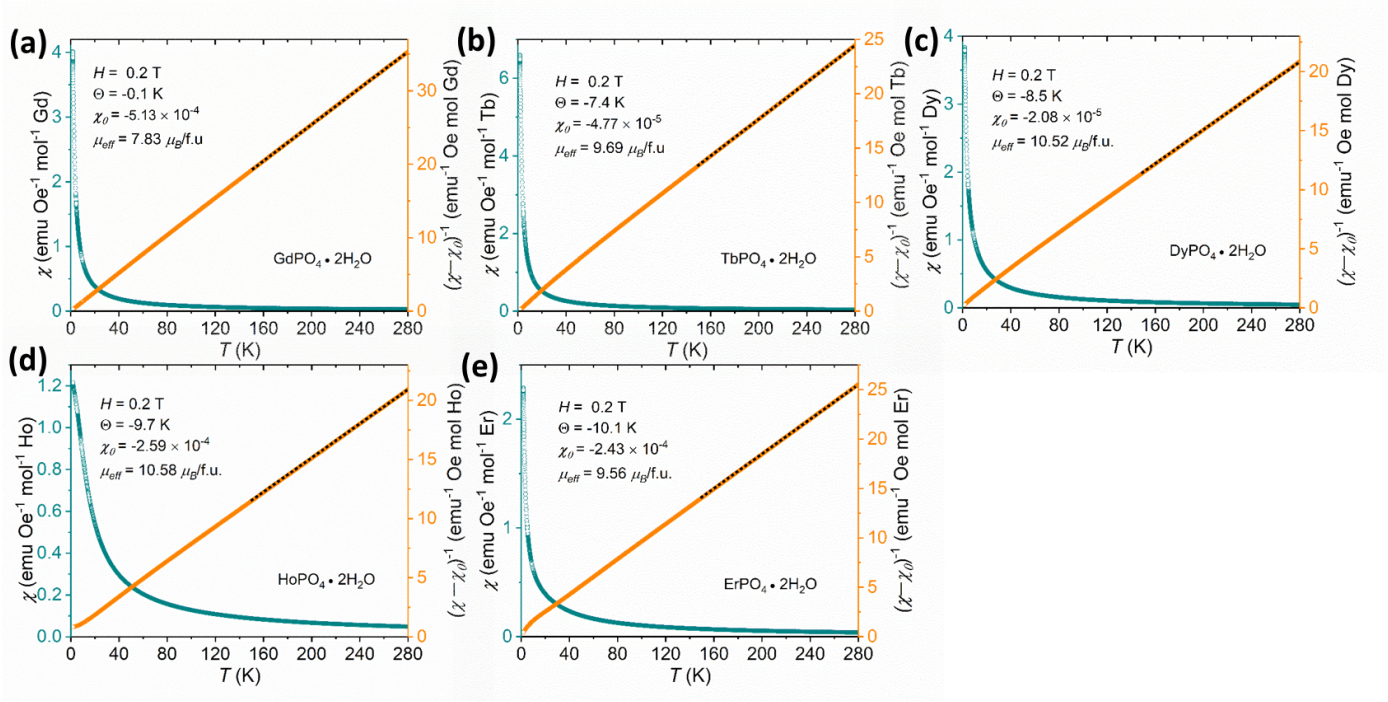
(a)
H = 0.2 T
Θ = -0.1 K
χ0 = -5.13 × 10-4
μeff = 7.83 μB/f.u
GdPO4 • 2H2O
χ (emu Oe-1 mol-1 Gd)
(χ−χ0)-1 (emu-1 Oe mol Gd)
T (K)
(b)
H = 0.2 T
Θ = -7.4 K
χ0 = -4.77 × 10-5
μeff = 9.69 μB/f.u
TbPO4 • 2H2O
χ (emu Oe-1 mol-1 Tb)
(χ−χ0)-1 (emu-1 Oe mol Tb)
T (K)
(c)
H = 0.2 T
Θ = -8.5 K
χ0 = -2.08 × 10-5
μeff = 10.52 μB/f.u.
DyPO4 • 2H2O
χ (emu Oe-1 mol-1 Dy)
(χ−χ0)-1 (emu-1 Oe mol Dy)
T (K)
(d)
H = 0.2 T
Θ = -9.7 K
χ0 = -2.59 × 10-4
μeff = 10.58 μB/f.u.
HoPO4 • 2H2O
χ (emu Oe-1 mol-1 Ho)
(χ−χ0)-1 (emu-1 Oe mol Ho)
T (K)
(e)
H = 0.2 T
Θ = -10.1 K
χ0 = -2.43 × 10-4
μeff = 9.56 μB/f.u.
ErPO4 • 2H2O
χ (emu Oe-1 mol-1 Er)
(χ−χ0)-1 (emu-1 Oe mol Er)
T (K)

Figure 10

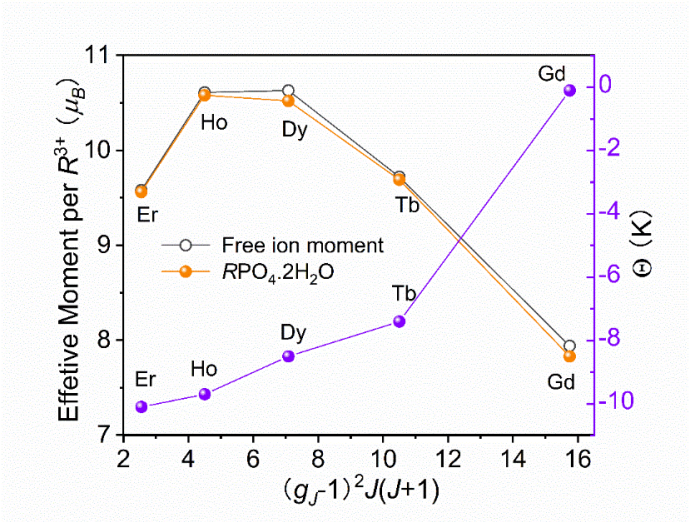
Effetive Moment per R^{3+} (μ_B)
Θ (K)
$(g_J\text{-}1)^2J(J+1)$
Free ion moment
$RPO_4.2H_2O$
Er
Ho
Dy
Tb
Gd
Er
Ho
Dy
Tb
Gd

Figure 11

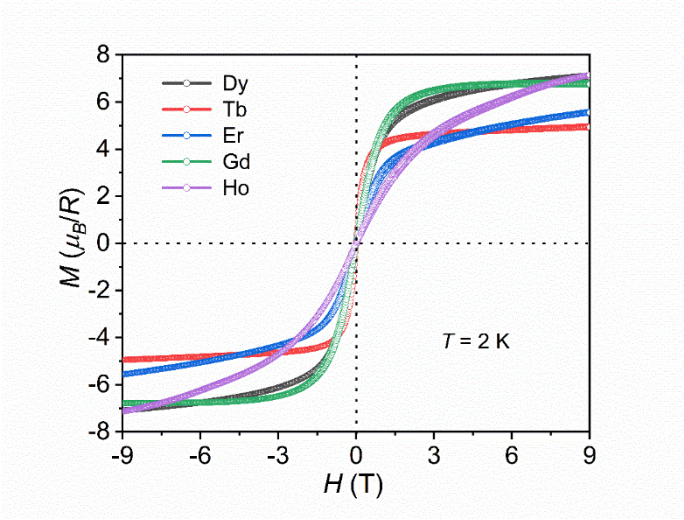

Figure 12

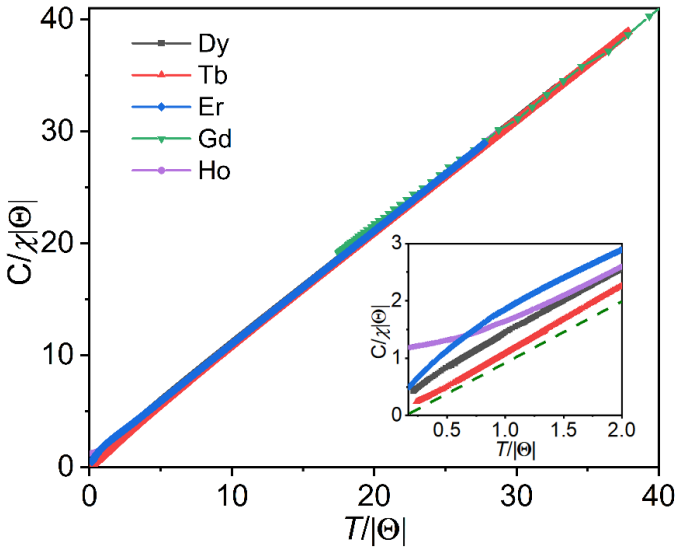

References

[1] A. Tymiński, T. Grzyb, Are rare earth phosphates suitable as hosts for upconversion luminescence? Studies on nanocrystalline REPO4 (RE=Y, La, Gd, Lu) doped with Yb3+ and Eu3+, Tb3+, Ho3+, Er3+ or Tm3+ ions, J. Lumin. 181 (2017) 411–420. doi:https://doi.org/10.1016/j.jlumin.2016.09.028.

[2] H. Onoda, H. Nariai, A. Moriwaki, H. Maki, I. Motooka, Formation and catalytic characterization of various rare earth phosphates, J. Mater. Chem. 12 (2002) 1754–1760. doi:10.1039/B110121H.

[3] N. Dacheux, N. Clavier, R. Podor, Monazite as a promising long-term radioactive waste matrix: Benefits of high-structural flexibility and chemical durability, Am. Mineral. 98 (2013) 833–847. doi:10.2138/am.2013.4307.

[4] F. Zhang, S.S. Wong, Ambient Large-Scale Template-Mediated Synthesis of High-Aspect Ratio Single-Crystalline, Chemically Doped Rare-Earth Phosphate Nanowires for Bioimaging, ACS Nano. 4 (2010) 99–112. doi:10.1021/nn901057y.

[5] Y. Ni, J.M. Hughes, A.N. Mariano, Crystal chemistry of the monazite and xenotime structures, Am. Mineral. 80 (1995) 21–26.

[6] A. Mesbah, N. Clavier, E. Elkaim, C. Gausse, I. Ben Kacem, S. Szenknect, N. Dacheux, Monoclinic form of the rhabdophane compounds: REEPO4·0.667H2O, Cryst. Growth Des. 14 (2014) 5090–5098. doi:10.1021/cg500707b.

[7] T. Subramani, M.R. Rafiuddin, A. Shelyug, S. Ushakov, A. Mesbah, N. Clavier, D. Qin, S. Szenknect, E. Elkaim, N. Dacheux, A. Navrotsky, Synthesis, Crystal Structure, and Enthalpies of Formation of Churchite-type REPO4·2H2O (RE = Gd to Lu) Materials, Cryst. Growth Des. 19 (2019). doi:10.1021/acs.cgd.9b00524.

[8] S.N. Achary, S. Bevara, A.K. Tyagi, Recent progress on synthesis and structural aspects of rare-earth phosphates, Coord. Chem. Rev. 340 (2017) 266–297. doi:https://doi.org/10.1016/j.ccr.2017.03.006.

[9] M.R. Rafiuddin, A.P. Grosvenor, A Structural Investigation of Hydrous and Anhydrous Rare-Earth Phosphates, Inorg. Chem. 55 (2016) 9685–9695. doi:10.1021/acs.inorgchem.6b01471.

[10] N. Clavier, R. Podor, N. Dacheux, Crystal chemistry of the monazite structure, J. Eur. Ceram. Soc. 31 (2011) 941–976. doi:10.1016/j.jeurceramsoc.2010.12.019.

[11] M.R. Rafiuddin, C. Tyagi, M. A. Haq, Synthesis and structural investigation of churchite-type REPO4·2H2O (RE = Y, Gd, Dy) nanocrystals, J. Solid State Chem. 311 (2022) 123150. doi:https://doi.org/10.1016/j.jssc.2022.123150.

[12] M. Guan, F. Tao, J. Sun, Z. Xu, Facile Preparation Method for Rare Earth Phosphate Hollow Spheres and Their Photoluminescence Properties, Langmuir. 24 (2008) 8280–8283. doi:10.1021/la800789x.

[13] C. Zhang, J. Chen, X. Zhu, Y. Zhou, D. Li, Synthesis of Tributylphosphate Capped Luminescent Rare Earth Phosphate Nanocrystals in an Ionic Liquid Microemulsion,

Chem. Mater. 21 (2009) 3570–3575. doi:10.1021/cm901061c.

[14] M.R. Rafiuddin, A.-M. Seydoux-Guillaume, X. Deschanels, A. Mesbah, C. Baumier, S. Szenknect, N. Dacheux, An in-situ electron microscopy study of dual ion-beam irradiated xenotime-type ErPO4, J. Nucl. Mater. 539 (2020) 152265. doi:https://doi.org/10.1016/j.jnucmat.2020.152265.

[15] C. Lenz, G. Thorogood, R. Aughterson, M. Ionescu, D.J. Gregg, J. Davis, G.R. Lumpkin, The Quantification of Radiation Damage in Orthophosphates Using Confocal μ-Luminescence Spectroscopy of Nd3+, Front. Chem. 7 (2019) 13. doi:10.3389/fchem.2019.00013.

[16] M.R. Rafiuddin, A.P. Grosvenor, Probing the effect of radiation damage on the structure of rare-earth phosphates, J. Alloys Compd. 653 (2015) 279–289. doi:10.1016/j.jallcom.2015.08.276.

[17] M.R. Rafiuddin, A.P. Grosvenor, An investigation of the chemical durability of hydrous and anhydrous rare-earth phosphates, J. Nucl. Mater. 509 (2018). doi:10.1016/j.jnucmat.2018.07.039.

[18] Y. Arinicheva, C. Gausse, S. Neumeier, F. Brandt, K. Rozov, S. Szenknect, N. Dacheux, D. Bosbach, G. Deissmann, Influence of temperature on the dissolution kinetics of synthetic LaPO4-monazite in acidic media between 50 and 130 °C, J. Nucl. Mater. (2018). doi:https://doi.org/10.1016/j.jnucmat.2018.07.009.

[19] C. Gausse, S. Szenknect, A. Mesbah, N. Clavier, S. Neumeier, N. Dacheux, Dissolution kinetics of monazite LnPO4 (Ln = La to Gd): A multiparametric study, Appl. Geochemistry. 93 (2018) 81–93. doi:https://doi.org/10.1016/j.apgeochem.2018.04.005.

[20] C. Liu, Y. Hou, M. Gao, Are Rare-Earth Nanoparticles Suitable for In Vivo Applications?, Adv. Mater. 26 (2014) 6922–6932. doi:https://doi.org/10.1002/adma.201305535.

[21] M.F. Dumont, C. Baligand, Y. Li, E.S. Knowles, M.W. Meisel, G.A. Walter, D.R. Talham, DNA Surface Modified Gadolinium Phosphate Nanoparticles as MRI Contrast Agents, Bioconjug. Chem. 23 (2012) 951–957. doi:10.1021/bc200553h.

[22] H. Saji, T. Yamadaya, M. Asanuma, Magnetic Properties of RXO4 System, J. Phys. Soc. Japan. 28 (1970) 913–920. doi:10.1143/JPSJ.28.913.

[23] A.H. Cooke, S.J. Swithenby, M.R. Wells, Magnetic interactions in holmium phosphate, $HoPO_4$, J. Phys. C Solid State Phys. 6 (1973) 2209–2216. doi:10.1088/0022-3719/6/13/019.

[24] G.A. Kumar, N.R. Balli, M. Kailasnath, L.C. Mimun, C. Dannangoda, K.S. Martirosyan, C. Santhosh, D.K. Sardar, Spectroscopic and magnetic properties of neodymium doped in GdPO4 sub-micron-stars prepared by solvothermal method, J. Alloys Compd. 672 (2016) 668–673. doi:https://doi.org/10.1016/j.jallcom.2016.02.165.

[25] N. Doebelin, R. Kleeberg, {\it Profex}: a graphical user interface for the Rietveld refinement program {\it BGMN}, J. Appl. Crystallogr. 48 (2015) 1573–1580. doi:10.1107/S1600576715014685.

[26] Y.F. Hu, L. Zuin, R. Reininger, T.K. Sham, VLS-PGM beamline at the Canadian light source, in: AIP Conf. Proc., 2007: pp. 535–538. doi:10.1063/1.2436116.

[27] B. Ravel, M. Newville, ATHENA, ARTEMIS, HEPHAESTUS: data analysis for X-ray absorption spectroscopy using IFEFFIT, J. Synchrotron Radiat. 12 (2005) 537–541. http://dx.doi.org/10.1107/S0909049505012719.

[28] S.M. Heald, D.L. Brewe, E.A. Stern, K.H. Kim, F.C. Brown, D.T. Jiang, E.D. Crozier, R.A. Gordon, XAFS and micro-XAFS at the PNC-CAT beamlines, J. Synchrotron Radiat. 6 (1999) 347–349. http://dx.doi.org/10.1107/S090904959801677X.

[29] L.S. Ivashkevich, A.S. Lyakhov, A.F. Selevich, PREPARATION AND STRUCTURE OF THE YTTRIUM PHOSPHATE DIHYDRATE, Phosphorus Res. Bull. 28 (2013) 45–50.

[30] M.R. Rafiuddin, E. Mueller, A.P. Grosvenor, X-ray Spectroscopic Study of the Electronic Structure of Monazite- and Xenotime-Type Rare-Earth Phosphates, J. Phys. Chem. C. 118 (2014) 18000–18009. doi:10.1021/jp5051996.

[31] H. Asakura, T. Shishido, K. Teramura, T. Tanaka, Local Structure and La L1 and L3-Edge XANES Spectra of Lanthanum Complex Oxides, Inorg. Chem. 53 (2014) 6048–6053. doi:10.1021/ic500381z.

[32] H. Asakura, T. Shishido, S. Fuchi, K. Teramura, T. Tanaka, Local Structure of Pr, Nd, and Sm Complex Oxides and Their X-ray Absorption Near Edge Structure Spectra, J. Phys. Chem. C. 118 (2014) 20881–20888. doi:10.1021/jp504507c.

[33] H. Asakura, S. Hosokawa, K. Teramura, T. Tanaka, Local Structure and L1- and L3-Edge X-ray Absorption Near Edge Structures of Middle Lanthanoid Elements (Eu, Gd, Tb, and Dy) in Their Complex Oxides, Inorg. Chem. (2021). doi:10.1021/acs.inorgchem.1c00151.

[34] A. Mesbah, N. Clavier, E. Elkaim, S. Szenknect, N. Dacheux, In pursuit of the rhabdophane crystal structure: from the hydrated monoclinic LnPO4.0.667H2O to the hexagonal LnPO4 (Ln = Nd, Sm, Gd, Eu and Dy), J. Solid State Chem. 249 (2017) 221–227. doi:https://doi.org/10.1016/j.jssc.2017.03.004.

[35] L.A. Boatner, Synthesis, Structure, and Properties of Monazite, Pretulite, and Xenotime, Rev. Mineral. Geochemistry. 48 (2002) 87–121. doi:10.2138/rmg.2002.48.4.